3

How Linear Motor Proteins Work

K. Oiwa[1] and D.J. Manstein[2]

[1] Kobe Advanced ICT Research Center (KARC), National Institute of Information and Communications Technology, 588-2 Iwaoka, Nishi-ku, Kobe 651-2492, Japan
[2] Institutes for Biophysical Chemistry and Structure Analysis, Hannover Medical School, OE4350, Carl-Neuberg-Straße 1, D-30623 Hannover, Germany

3.1 Introduction

Most animals perform sophisticated forms of movement such as walking, running, flying and swimming using their skeletal muscles. Although directed movement is not generally associated with plants, cytoplasmic streaming in plant cells can reach velocities greater than 50 μm/s and thus constitutes one of the fastest forms of directed movement. Unicellular eukaryotic organisms and prokaryotes display diverse mechanisms by which they are able to actively move towards a food source, light or other sensory stimuli. On the cellular level active transport of vesicles and organelles is required, since the cytoplasm resembles a gel with a mesh size of approximately 50 nm, which makes the passive transport of organelle-sized particles impossible. For elongated cells such as neurons, even proteins and small metabolites have to be actively transported.

Linear motor proteins, moving on cytoskeletal filaments such as actin filaments and microtubules, are predominantly responsible for the motile activity in eukaryotic cells. They are chemo-mechanical enzymes that use the chemical energy from adenosinetriphosphate (ATP) hydrolysis to generate force and to move cargoes along their filament tracks. Under physiological conditions, the energy input per molecule of ATP corresponds to the chemical free energy liberated by its hydrolysis to adenosinediphosphate (ADP) and inorganic phosphate (P_i), ca. 10^{-19} J (100 pNnm). The thermodynamic efficiency of motor proteins varies between 30 and 60%. As machines, motor proteins are unique since they convert chemical energy to mechanical work directly, rather than through an intermediate such as heat or electrical energy.

3.2 Structural Features of Cytoskeletal Motor Proteins

Three families of linear, cytoskeletal motor proteins have been described: kinesin, dynein, and myosin (Fig. 3.1). Kinesin and dynein family members

K. Oiwa and D.J. Manstein: *How Linear Motor Proteins Work*, Lect. Notes Phys. **711**, 41–63 (2007)
DOI 10.1007/3-540-49522-3_3

move along microtubules while the members of the extended myosin superfamily move along actin filaments. The number of molecular engines and motor proteins has greatly increased with the advance of the various genome projects. We now know more than eighteen myosin subfamilies or classes. Thirty-nine myosin heavy chain genes have been found in the human genome; nine of these are expressed in muscle tissues, while the remainders, the so-called unconventional myosins, are responsible for cell motilities other than muscle contraction. Fourteen subfamilies are known for kinesins and three for dyneins.

Comparisons of the available full-length sequences of dynein heavy chains have shown that dynein is a member of the AAA^+ (ATPase Associated with various cellular Activities) protein family [1]. So far, more than 200 AAA^+ family members have been identified that participate in diverse cellular processes. Dyneins are further divided into two groups: cytoplasmic dynein and axonemal dynein. Cytoplasmic dynein is composed of two identical heavy chains of about 530 kDa each. Additionally, cytoplasmic dyneins consist of two 74 kDa intermediate chains, about four 53–59 kDa intermediate chains, and several light chains. Axonemal dynein shares the same heavy chain structure but its overall structure is far more complicated and will not be discussed here in detail (reviewed in [2]).

Dynein heavy chains consist of the C-terminal head with two elongated flexible structures called the stalk (microtubule-binding domain) and the N-terminal tail (cargo-binding domain). The head and the stalk form a motor domain (Fig. 3.1d). The motor domains of all dyneins are generally well conserved in sequence (with 40–80% similarity) [3] and are indistinguishable by electron microscopy at the single-particle level (reviewed in [4]). A single dynein motor domain has a mass of almost 380 kDa. Most of this mass is contained in seven protein densities that encircle a cavity to produce a ring-like architecture, named a head ring. At least six of the seven densities probably correspond to the highly conserved AAA-modules containing specialized motifs for ATP binding (e.g. P-loop motif). The first four of six AAA-modules are predicted to bind nucleotides [5]. The first P-loop (P1) has the most highly conserved sequence among dyneins and was previously assigned as the principal site of ATP hydrolysis by vanadate-mediated photocleavage of the dynein heavy chain. Further strong support for a functional role of P1 has been provided by molecular dissection of cytoplasmic dyneins in which mutation of this P-loop abolished motor activitiy [4, 6]. The microtubule binding domain named the stalk, is flanked by two relatively long coiled-coil regions and is structurally conserved among all dyneins. This stalk extends from the head between AAA-modules #4 and #5. Its tip interacts with microtubules in an ATP-sensitive manner.

Based on electron microscopic observation of an axonemal dynein, our group proposed a model in which multiple conformational changes are coordinated in such a way that the changes between the AAA domain #1 and its neighbors are amplified by the docking of the head ring onto a linker that

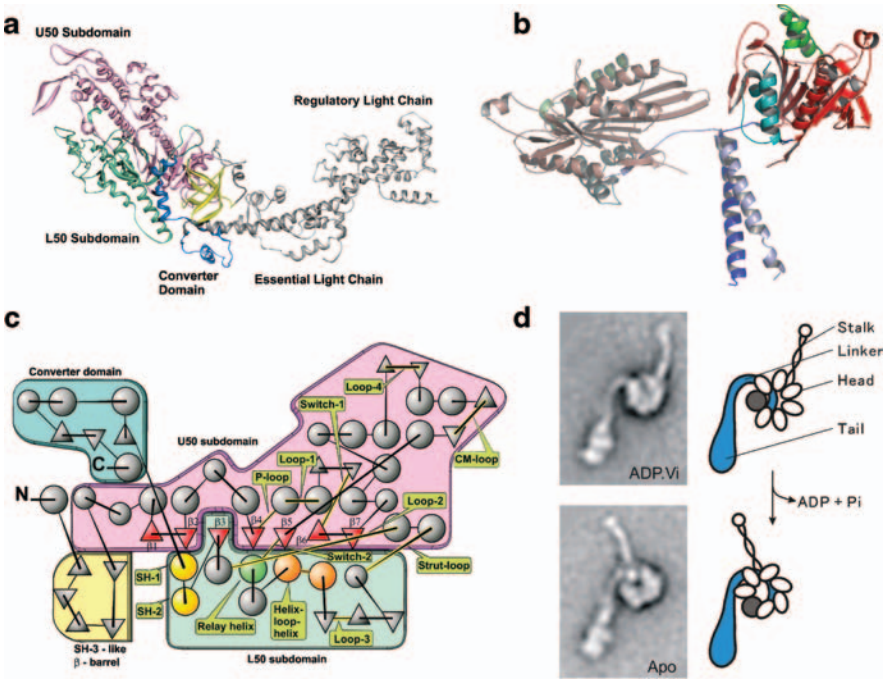

Fig. 3.1. Structure and topology of molecular motors. (**a**) Structure of the myosin motor domain with light chain binding region. N-terminal domain, green; L50 or actin binding domain, cyan; U50, red; C-terminal domain, blue. The essential and regulatory light chains are colored yellow and magenta, respectively. (**b**) Structure of the kinesin 1 motor domain dimer. Switch-1 region, green; switch-2 region, cyan; neck linker and neck helix, blue. (**c**) Topological map of the myosin motor domain. In addition to the domains and subdomains shown, crystallographic results reveal that the segment between $\beta 7$ and switch-2 moves as a solid body and can be regarded as an independent subdomain. Helices are shown as *circles* and β-strands as *triangles*. The background colours are: N-terminal SH3-like β-barrel, yellow; U50 subdomain, pink; L50 subdomain, cyan; converter domain, light-blue. The 7-stranded central β-sheet is shown in red ($\beta 1$ 116–119; $\beta 2$ 122–126; $\beta 3$ 649–656; $\beta 4$ 173–178; $\beta 5$ 448–454; $\beta 6$ 240–247; $\beta 7$ 253–261) (modified from [7]). (**d**) Isolated molecules of a monomeric flagellar inner arm dynein (subspecies c), imaged in two biochemical states using negative staining electron microscopy. These images show that the ADP.Vi-molecule has the same general form as the apo-molecule, but the latter is more compact. Schematic diagram of the power stroke of axonemal dynein. Rigid coupling between AAA domain #1 and a linker causes a rolling of the head towards the tail which translates the microtubule by 15 nm under zero load conditions. The distance between the tip of the stalk in these two conformations is approximately 15 nm [8]

connects the tail and the head ring [8] (Fig. 3.1d). When the stalk tip binds tightly to a microtubule, this may promote a concerted conformational change in AAA-modules #4 to #1, leading to activation of release of ADP and phosphate from AAA-module #1. Rigid coupling between AAA-module #1 and linker causes a rolling of the head towards the stem. The linker docks on the head ring and the resultant rotation of the head ring swings the stalk. Judging from the sequence and structural similarities between axonemal and cytoplasmic dyneins, it appears reasonable to assume that the two dynein subfamilies adopt the same mechanism for force generation.

Kinesin [9,10] and myosin [11] motor domains share a common core structure even though they move on different filament tracks and the myosin motor domain is twice as large as the ∼350 residue kinesin motor domains (Fig. 3.1a, b). The core structure of kinesin and myosin motor domains is distantly related to the GTPase subunit of heterotrimeric G proteins and small G-proteins of the Ras family [12, 13]. The core structure includes three conserved sequence motifs, termed P-loop, switch-1 and switch-2 at the nucleotide-binding pocket, which act as γ-phosphate sensors. Their switching between ATP and ADP states is associated with specific intramolecular movements, analogous to the nucleotide dependent conformational transitions in G-proteins, which are central to the mechanism of kinesin and myosin family motors. To carry out directed movements, motor proteins must be able to associate with and dissociate from their filament tracks. All motor proteins have at least one force-producing motor domain that contains in addition to the active site, which is responsible for ATP binding and hydrolysis, a binding site for the cytoskeletal filament. In myosins and conventional kinesin, a neck domain connects the motor domain to the tail region. The neck region of myosins is formed by one or more so-called IQ motifs serving as binding sites for calmodulin or calmodulin-like light chains (Fig. 3.1a). The resulting complex of extended α-helical heavy chain and tightly bound light chains serves as a lever arm amplifying and redirecting smaller conformational changes within the myosin motor domain that occur during the interaction with nucleotide and filamentous actin (F-actin) [14,15]. The cargo-binding tail domain shows high diversity both between motor families and within a single motor family. This enables different motors to bind different cargoes and thus to perform a wide variety of cellular functions.

3.3 In Vitro Motility Assays: A Link between Physiology and Biochemistry

A key issue in motor protein research is the mechanism of chemomechanical coupling. For myosin, we would like to understand how a series of chemical events such as ATP binding, hydrolysis of ATP, release of phosphate, and ADP release induce changes in the ATP binding site, and how the changes

are coupled to events at the actin binding site and transmitted into large scale structural changes leading to the production of working strokes of 5 to 50 nm.

Detailed structural information is required to unravel the mechanism by which force and movement are produced. In addition, to link the enzyme kinetics of the motor protein ATPase in solution with the mechanics and energetics of motor proteins, it is essential to use experimental systems in which both ATP-turnover and mechanical parameters can be accurately measured. Here, motor protein studies were advanced greatly by the development of in vitro motility assays. In such assays, the motility of a system consisting only of the purified motor protein, F-actin or microtubules, ATP and buffer solution can be measured under well-defined conditions. The in vitro assay systems are useful in filling the gap between the physiology and biochemistry of motor proteins because these systems enable us to directly observe force generation and movement involving only a very small number of protein molecules.

Two typical geometries are used for in vitro motility assays: bead assays and surface assays (Fig. 3.2). In the former, filaments are fixed to a substrate, such as a microscope slide, and motors are attached to small plastic beads, typically 1 μm in diameter, or to the tip of a fine glass needle. The motion of the beads or of the needle along the filaments in the presence of ATP is visualized using a light microscope. Position and movement of the beads or the needle are measured photo-electrically and can be determined with a resolution on the order of nanometers and sub-millisecond time-response. In the surface assays, the motors themselves are fixed to the substrate, and filaments are observed to diffuse down from solution, attach to and glide over the motor-coated surface. Visualization of the filaments is readily accomplished using dark-field or fluorescence microscopy. Measurements performed on large numbers of enzyme molecules frequently hide important details of their mechanism. Similarly, the discrete actions performed by individual motor proteins are buried in the average when the net output from a large number of asynchronous motors is monitored. In recent decades, rapid progress in a number of technologies such as atomic force microscopy, optical trap nanometry and fluorescence microscopy has provided us with tools to follow the dynamics of single-molecules in situ with spatial and temporal resolution extending to the Å and μs ranges. This allows the direct observation of the dynamic properties of molecular motors, which macroscopic ensemble-averaged measurements cannot detect. Two fundamental motor protein parameters, coupling efficiency and step-size, that can only be indirectly inferred from conventional in vitro motility assays are now accessible by single molecule approaches, permitting the direct and simultaneous observation of ATP-turnover and force production.

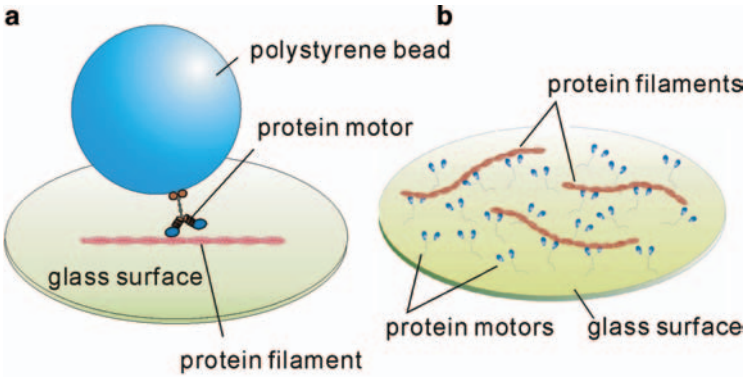

Fig. 3.2. Geometries for quantitative in vitro motility assays. (**a**) Motile activity can be detected and quantified by attaching the motor to a bead and allowing it to interact in an ATP-dependent manner with microtubules or oriented actin filaments on the cover glass surface. (**b**) Alternatively, individual fluorescence labelled and phalloidin-stabilized actin filaments can be observed moving over a lawn of myosins and microtubules can be observed moving over a lawn of dynein or kinesin motors

3.4 Structural Features of the Myosin Motor Domain

The core of the myosin motor domain is formed by a central, 7-stranded β-sheet and is surrounded by α-helices (Fig. 3.1a). The N-terminal 30 residues of the myosin heavy chain extended between the motor domain and the neck region. Unless otherwise stated, sequence numbering refers to the *Dictyostelium* myosin-II heavy chain. Residues 30–80 form a protruding SH3-like β-barrel domain. The function of this small domain is unknown; however, it is absent in class-I myosins and thus appears not to be essential for motor activity. A large structural domain, which accounts for 6 of the 7 strands of the central β-sheet, is formed by residues 81–454 and 594–629 (Fig. 3.1c). This domain is usually referred to as the upper 50K domain (U50). A large cleft divides the U50 from the lower 50K domain (L50), a well defined structural domain formed by residues 465–590. The actin binding region and nucleotide binding site of myosin are on opposite sides of the seven-stranded β-sheet and separated by 40–50 Å. The P-loop and the switch motifs are located in the U50 domain and form part of the ATP binding site. Switch-1 and switch-2 contact the nucleotide at the rear of the nucleotide binding pocket. The switch motifs move towards each other when ATP is bound and move away from each other in its absence. Conformational changes during the transition between different nucleotide states do mostly correspond to rigid-body rotations of secondary and tertiary structure elements. The motor domain can thus be regarded as consisting of communicating functional units with substantial movement occurring in only a few residues.

Residues 630–670 form a long helix that runs from the actin binding region at the tip of the large cleft to the 5th strand of the central β-sheet. A turn and

a broken helix are formed by residues 671–699. The segments of the broken helix are frequently referred to as SH1 and SH2-helices. The converter domain formed by residues 700–765 functions as a socket for the C-terminal light chain binding domain and plays a key role in the communication between the active site and neck region.

3.5 Amplification of the Working Stroke by a Lever Arm Mechanism

According to the lever arm model, the step size of myosins is predicted to be proportional to the length of the neck region. An important feature of the lever arm model is that it has the neck region rigidly attached to the converter domain. During the power stroke, converter domain and lever arm swing together in a rigid body motion (Fig. 3.3a). The axis of rotation lies close to and is oriented almost parallel to a long α-helix formed by residues 466–496, which is usually referred to as the relay helix (Fig. 3.1c). The swinging movement, from an initial *UP* position to a *DOWN* position at the end of the working-stroke, is accompanied by the release of the hydrolysis products inorganic phosphate and ADP. The actomyosin ATPase cycle (Fig. 3.4) can be described by a number of intermediate states, which have ATP, its hydrolysis products or no nucleotide bound at the active site and display high or low affinity for F-actin.

The ATP-bound and nucleotide-free states are structurally and biochemically well-defined. They define extreme positions in regard to nucleotide and actin affinity as well as lever arm position. In the ATP-bound state, the affinity of myosin for F-actin is 10,000-fold reduced compared to the nucleotide-free protein. Conversely, strong binding to F-actin reduces the affinity for nucleotide 10,000-fold. The following sequence of events explains the reciprocal relationship between actin and nucleotide affinity. The switch-1 loop preceding $\beta 2$, the switch-2 loop following $\beta 3$, and the P-loop following $\beta 4$ undergo large conformational changes upon ATP-binding. These movements of the active site loops stabilize γ-phosphate binding and the coordination of the Mg^{2+} ion. Additionally, the three edge β-strands: $\beta 5, \beta 6$, and $\beta 7$ change their orientation, which leads to large changes in the relative position of the U50 and L50 subdomains and opening of the large cleft between them. Changes of nucleotide binding loop structures are thereby coupled to large movements of the actin binding region. The central role played by the interaction between γ-phosphate and nucleotide-binding loops explains why ATP but not ADP can induce the changes leading to low actin affinity. The establishment of a tight network of hydrogen bonds in the final ATP-myosin complex is concomitant with the formation of a proper active site. This allows the ATPase cycle to advance to the myosin-ADP-P_i intermediate. However, ATP hydrolysis is not the key step that drives the cycle forward. In fact the equilibrium constant for the hydrolysis step is close to unity. What makes the cycle unidirectional

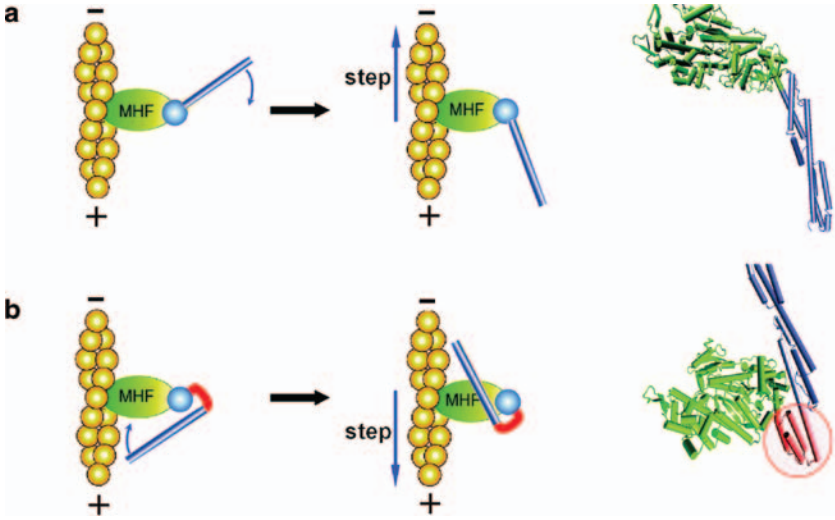

Fig. 3.3. Mechanical models for myosin-based forward and backward movement. (**a**) Power-stroke of a conventional barbed plus-end directed myosin. (**b**) The insertion of a domain (*red*) between the converter region (*blue*) and the lever arm (*orange*) reverses the direction of the power-stroke and produces a minus-end directed myosin. The lever arm moves tangential to the long axis of the actin filament. The right hand panels show the myosin motor domain in the post power-stroke state (*green*) with an artificial lever arm consisting of two α-actinin repeats (*blue*) or two α-actinin repeats and a directional inverted that is derived from the hGBP 4-helix bundle (*red*)

is the irreversibility of ATP binding. Binding of the myosin motor domain to actin induces a reversal of the sequence of conformational changes that are induced by ATP binding. Strong actin binding induces closing of the large cleft between U50 and L50 [16]; this leads to a distortion of the central β-sheet, the outward movement of the nucleotide binding loops disrupts the coordination of the Mg^{2+} ion and thereby ADP binding [17, 18]. The loss of the Mg^{2+}-ion coordination induced by actin-binding is similar to the effect of GTPase exchange factors on the release of GDP by small G-proteins. Therefore, actin can be viewed as an ADP-exchange factor for myosin [12, 18]. Concomitant with the transition from the ATP-bound state to the rigor-like state, the lever arm swings from its *UP* position to the *DOWN* position [19].

The various genome projects have led to the identification of a large number of new myosins and myosin classes. However, their characterisation is greatly impeded by the fact that the sequencing projects cannot identify the light chains that are associated with the individual myosin heavy chains. In the case of class-I myosins, analysis of the motor activity of the native protein is further hampered by the presence of an ATP-insensitive actin-binding site in the tail region [20]. Here, the direct fusion of an artificial lever arm to

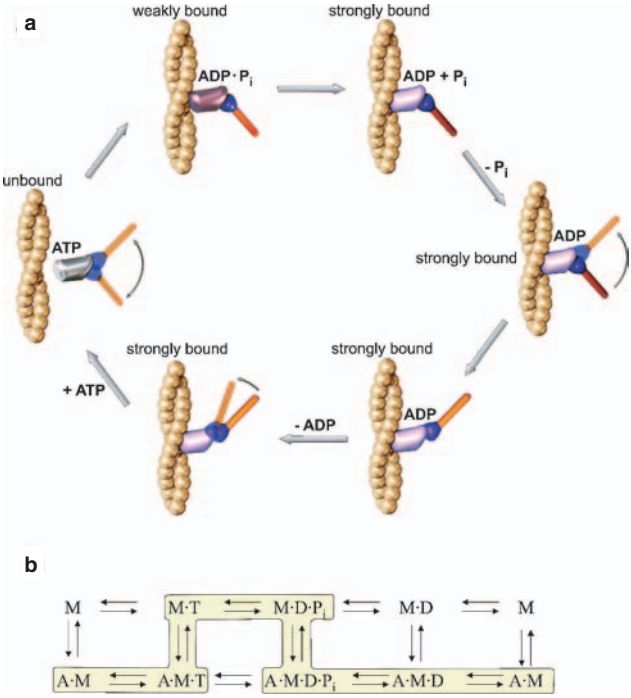

Fig. 3.4. Actomyosin ATPase cycle. (*Upper panel*) Mechanochemical scheme of the actomyosin ATPase cycle. Actin monomers are shown as golden spheres. The motor domain is colored metallic grey for the free form, purple for the weakly-bound form, and violet for the strongly-bound form. The converter is shown in blue and the lever arm in orange. Starting from the *top-right* the following sequence of events is shown: ATP binding induces dissociation of the actomyosin complex. The lever arm returns in the pre-powerstroke position and ATP hydrolysis occurs. Actin-binding can be described in terms of a three-state docking model. The initial formation of a weakly bound collision complex between the myosin head and F-actin is governed by long range ionic interactions and is strongly dependent on ionic strength but independent of temperature. Strong binding is initiated by the following isomerisation to the A-state, leading to the formation of stereospecific hydrophobic interactions. The A-state is affected by organic solvent and temperature. Ionic strength has a comparatively small effect on the formation of this state. The following stepwise transition upon P_i release and then ADP release to a strongly bound state (R-state) involves major structural rearrangements with formation of additional A-M contacts. The conformational changes involve both hydrophobic and ionic interactions. In many myosins both P_i and ADP release result in movement of the lever arm and contribute to the working stroke. The A-to-R transition is dependent on the effective concentration of F-actin and hydrolysis products, as the reaction sequence is readily reversible [21]. (*Lower panel*) Minimal description of the myosin and actomyosin ATPase as defined in solution. *Vertical arrows* indicate the actin association and dissociation from each myosin complex. In every case the events shown can be broken down into a series of sub steps involving one or more identifiable protein conformational changes. The states with a *yellow* background represent the predominant pathway for the actomyosin ATPase (modified from [7])

the motor domain greatly facilitates the production and characterization of recombinant myosin motors displaying full motile activity. It could be demonstrated that the kinetic properties of myosin motor domains from various classes are not affected by the fusion with an artificial lever arm [22, 23]. The replacement of the native neck region with artificial lever arms is facilitated by the limited number of contacts between the motor domain and the neck region. The main technical problems that need to be overcome are the creation of a stiff junction and tight control over the direction in which the lever projects away from the motor domain. Spectrin-like repeats have been used to produce constructs with artificial lever arms of different length for a variety of unconventional myosins.

We applied this approach to characterize the motor properties of a myosin XI, which drives cytoplasmic streaming [22]. Cytoplasmic streaming, as found in plant cells and algae, belongs with velocities of up to 100 μm s^{-1} to the fastest forms of actin-based motility. Electron microscopy of rotary shadowed native plant myosin XI show two head domains with elongated neck regions that are much larger than those observed with myosin II. The neck regions join in a thin stalk of 25 nm length, which has two smaller globular domains attached to its distal end. This structural organization is similar to that of myosin V, whose mechanical properties have been extensively studied [24]. A *Chara corallina* myosin XI motor domain fused to two α-actinin repeats, corresponding to an artificial lever arm of approximately 12 nm length, moves actin filaments with a mean velocity of 16.2 μm/s in the in vitro motility assay [22, 25].

3.6 Backwards Directed Movement

Actin filaments are formed from G-actin monomers and microtubules from α/β-tubulin dimers. Due to the head-to-tail arrangement of these constituent building blocks, the resulting filaments are polar structures. The inherent polarity of the filaments and the stereospecificity of their interactions with motor proteins form the basis for directional movement in biological systems. Each individual type of motor protein moves towards either the plus or the minus end of its respective filament. The difference in the polymerization rates distinguish the fast-growing plus-ends from the slower-growing minus-ends. The directionality of a motor protein can be readily determined by in vitro motility assays. The minus-end of an actin filament or a microtubule can be fluorescently labeled to distinguish it from the plus-end. Using this technique, it was discovered that, different from conventional kinesin, the kinesin-related protein motors ncd [26] and Kar3 [27] are minus-end-directed microtubule-based motors and, different from conventional myosin, myosin VI [28, 29] and myosin IX [30] are minus-end directed actin-based motors.

Structural studies have shown that the myosin power-stroke occurs tangentially to a circle that is defined by the circumference of the actin filament

(reviewed in [31]). As described above, the origin of the translational movement of the lever arm is the rotation of the converter domain that results from the conformational changes associated with ATP-binding, ATP-hydrolysis, release of products and the interactions with F-actin. A lever arm mechanism implies that a reversal of the direction of movement can be achieved simply by rotating the attachment point of the lever arm through 180°. If the lever arm points in the opposite direction, the same rotation of the converter region that produces plus-end directed movement in the native myosin will lead to the opposite translational movement of the tip of the lever arm and therefore minus-end directed movement in the mutant constructs (Fig. 3.3) [32].

The following points need to be considered in engineering a construct with a lever arm rotated by 180°. First, a suitable protein or protein domain needs to be identified whose insertion leads to a near 180° rotation of the lever arm. Secondly, steric clashes between the lever arm and the motor domain must be avoided. Finally, rigid junctions have to be created and the individual building blocks joined in the proper orientation. The following molecular building blocks were used for the generation of an artificial minus-end directed myosin: a directional inverter formed by a 4-helix bundle motif derived from human guanylate binding protein-1 (hGBP), an artificial lever arm formed by *Dictyostelium* α-actinin repeats 1 and 2, and a plus-end directed class I myosin motor domain derived from *Dictyostelium* MyoE [32]. The design of a functional construct was considerably facilitated by the fact that the structures of all three building blocks used for the generation of the backwards-moving motor were known [33–35].

3.7 Surface-Alignment of Motor Proteins and their Tracks

The controlled attachment of motor proteins and their protein tracks to well-defined surface areas offers a potential route to the production of functional nanomachines. To this end, effective and non-destructive methods have been investigated for immobilizing these proteins on surfaces and for steering the resulting output in the form of force and movement in defined directions. Additionally, the motion of the protein filaments or beads needs to be under tight directional control and not random as in the standard in vitro assay system [36].

Microtubules have a low affinity for clean glass, but modifications of the glass surface can provide selective attachment of microtubules. Immobilizing microtubules selectively on lithographically patterned silane surfaces was first reported by [70]. They found that microtubules bound strongly to amine-terminal silanes while retaining the ability to act as active rails for kinesin motility. By exposing the silane surface to light from a deep UV laser, they produced aminosilane patterns lithographically with line widths varying from 1 to 50 μm, and used these patterns for selective adhesion of microtubules.

Using microtubules oriented by buffer flow and immobilized with aminosilane, [37] demonstrated that kinesin-coated silicon microchips can move across the microtubule surface. In these experiments microtubules were aligned along the patterns but not with equal polarity.

Alignment of protein tracks, microtubules or actin filaments with the same polarity is fundamental to applications of motor proteins as elementary force generators in nanotechnology. When driven by very small number of kinesin molecules, microtubules aligned under continuous buffer flow with the same polarity during active sliding [38]. However, the unipolar alignment of microtubules is quickly abolished by thermal agitation after cessation of the flow. Improving this technique, Böhm and coworkers (2001) immobilized microtubules aligned in buffer flow on kinesin-coated surface with gentle treatment with 0.1% glutardialdehyde. Even with this glutardialdehyde treatment, microtubules retained their activities as substrate for kinesin motility. Kinesin-coated beads (glass, gold and polystyrene) with 1–10 μm diameters moved unidirectional on the microtubules with average velocity of 0.3–1.0 μm s^{-1} over a distance up to 2.2 mm [39].

A simple and versatile method used in our laboratory for arranging microtubules on a glass surface in a defined array with uniform polarity uses positively charged nanometer-scale polyacrylamide beads and directional buffer flow [11]. Polarity-marked microtubules attached via their seed-end to the bead-surface even at high ionic strength. The seed-ends, which are located at the minus-end of the microtubules, contain ethylene glycol bis [succinimidyl-succinate] (EGS) cross-links and tetramethylrhodamine at a much higher concentration than the rest of the microtubule. Without EGS-crosslinking, the seed part does not bind to surfaces at high ionic strength. Low ionic strength solution is then introduced in the flow-cell and microtubules are directionally aligned in the direction of buffer flow (Fig. 3.5). Microtubules bind to beads tightly at low ionic strength. Generally, surface binding of microtubules is ionic strength-dependent and fully reversible. Surface-bound microtubules support normal movement of kinesin-coated beads in one direction, indicating that microtubules remain intact even after binding to the surface. The convenience of this procedure for orienting microtubules with uniform polarity makes these surfaces useful not only for powering nanometer-scale devices but also for measuring spectroscopic properties of microtubule motors, such as kinesin and dynein.

3.8 Controlling the Direction of Protein Filament Movement Using MEMS Techniques

The gliding movement of microtubules or actin filaments is now spatially controllable. A number of methods for the control of filament movement in defined directions have been developed. In these methods, chemical modifications and micro-fabrications of the surface have been used. In order to control the track

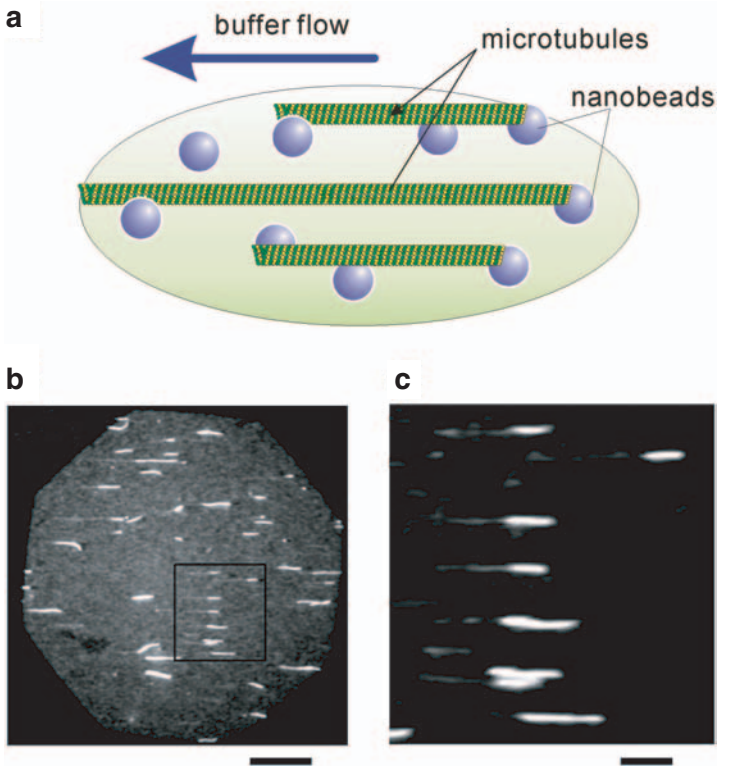

Fig. 3.5. Polarity-marked microtubules attached on positively-charged glass surface. (**a**) Illustration of experimental arrangement of nanobeads and seeds of microtubules. The glass surface was first coated with positively-charged polyacrylamide nanobeads. Since the EGS-cross linked seeds of microtubules (*bright fluorescence*) had negative charges, microtubules selectively attached on the surface at their minus ends. Buffer flow oriented these microtubules on the surface. (**b**, **c**) Fluorescence microscopic observation of aligned microtubules. The polarity of microtubules can be easily identified from the position of the brightly labeled seeds. The images demonstrate how microtubules can be efficiently aligned in a unipolar fashion by buffer flow. Scale bar, 15 μm in b, 4 μm in c

along which filaments glide, it is necessary to restrict the location of active motors to specific regions of the surface. While the detailed interactions of motor proteins with surfaces are not well understood, it has been observed that myosin motility is primarily restricted to the more hydrophobic resist surfaces [40, 41]. Thus, myosin and proteolytic fragments of myosin can be readily aligned on polytetrafluoroethylene (PTFE)-deposited surfaces, resulting in the movement of actin filaments being restricted to the well-defined fabricated tracks [42]. PTFE thin films are readily generated by rubbing a heated glass-coverslip surface with a PTFE rod while applying a defined

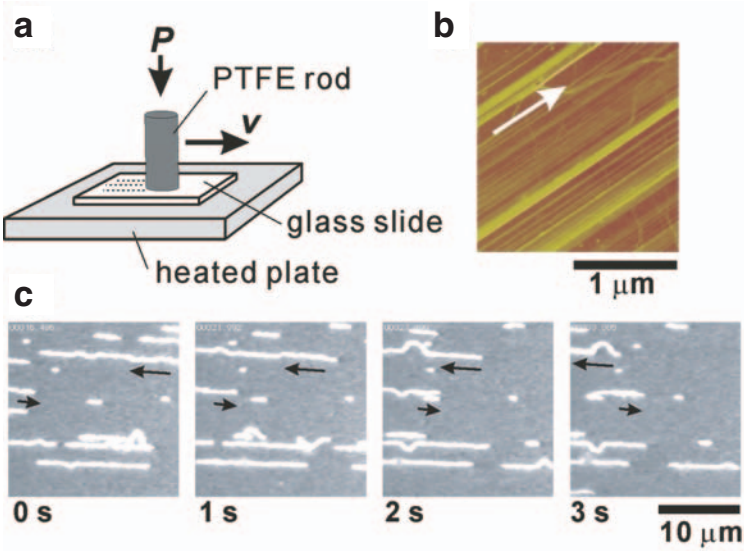

Fig. 3.6. Alignment of myosin or proteolytic fragments of myosin on polytetrafluoroethylene (PTFE)-deposited surfaces. (**a**) Mechanical deposition of PTFE thin film on glass surface. A rod of solid PTFE is moved against a coverslip on a hot plate at a constant rate of 50 mm/s and constant pressure (7×10^4 Pa). (**b**) Atomic force microscopic observation of the PTFE thin film deposited on the glass surface. (**c**) A sequence of fluorescence microscopy images showing the movement of fluorescent actin filaments on a myosin S1-coated PTFE-thin film. Actin filaments are moving on the ridges of the PTFE deposit in a bi-directional fashion. Reproduced with permission from [43]

pressure [44]. The PTFE thin films were used for alignment or graphoepitaxial crystal growth of a variety of substances [44, 45]. The resulting films on the coverslip surface consist of many linear and parallel PTFE ridges of 10–100 nm width (Fig. 3.6). Myosin or its proteolytic fragments, subfragment 1 (S1) or heavy meromyosin (HMM) bind to the ridges without losing activity and actin filaments move on these ridges with the speed that is typical for in vitro motility of myosin or myosin-fragment. This PTFE technique was also used for the kinesin-microtubule system [46].

However, the widths, heights and shapes of the PTFE ridges are difficult to control. To overcome this difficulty, various polymers were examined for use as surface coating, and several effective polymers that maintain the activity of motor proteins have been reported. Thus methods have been developed in which a glass or silicone surface is coated with resist polymers such as polymethylmethacrylate (PMMA) or SAL601. UV radiation, electron beams or soft lithography are then used to remove resist from defined regions and to draw specific patterns on the substrate. With careful selection of the buffer solutions [e.g. pH, ionic strength, concentration of motors, choice of

blocking substances such as casein and bovine serum albumin (BSA) and/or detergents], motility can be restricted either to the unexposed, resist polymer surface or to the exposed underlying substrate.

PMMA was the first resist polymer found to be useful for immobilizing myosin molecules while retaining their abilities to support the movement of actin [42]. Patterned surfaces were prepared by photolithography with PMMA-coated glass coverslip. Various patterns of tracks of PMMA were fabricated on coverslips, and HMM was introduced and immobilized on the patterns. Fluorescent actin filaments were then added in the presence of ATP. Their movements were confined to the PMMA tracks (Fig. 3.7). Through the study of the behavior of actin filaments moving in PMMA tracks, we found that the probability of an actin filament making a U-turn is low within a track of a few micrometers width. In addition, actin filaments often moved along the edges of the tracks when they approached the edge at low angles instead of escaping from the tracks. Thus, simple patterns can effectively bias the movement of actin filaments, confining them to unidirectional movement (Fig. 3.7c) [47].

In the experiments described above, the PMMA tracks are raised above the surrounding glass surface. This leads to actin filaments running off the tracks and their number gradually decreasing over time. Given the potential applications of this system, it is thus necessary to develop a way to restrict the movement of filaments to one dimension along linear tracks for extended periods of time. Restricting kinesin-driven movement of microtubules along linear tracks was achieved by using micrometer-scaled grooves lithographically fabricated on glass surfaces [48–50]. In the presence of detergent, kinesin selectively adsorbed onto a glass surface from which the photoresist polymer has been removed, not on the photoresist polymer itself [50]. The tracks thus have a reversed geometry as compared with those used previously i.e. they were channels bordered by walls of the resist material. Microtubules rarely climbed up the walls and moved away from the track. Therefore this method allowed us to limit the kinesin-driven movement of microtubules effectively to one dimension along a linear track. The sidewall collisions described above and the subsequent guidance of microtubules along the sidewall were well characterized by [49]. Similar nano-structured surfaces were also used for the actomyosin system [40] although actin filaments often climbed up the wall and escaped from tracks owing to their lower flexural rigidity compared with microtubules. This limitation has been overcome by shaping the surface morphology with nanometer precision, which forces the filaments to move exclusively on the tracks [51].

While it is possible to use chemical and topographical patterning to guide protein filaments and restrict their movement to particular tracks, it is more difficult to control the direction of movement along the track. The difficulty arises because the orientation in which motors bind to a uniform surface is not well controlled. The conversion of bidirectional movement into unidirectional movement along the linear tracks was finally accomplished by simply

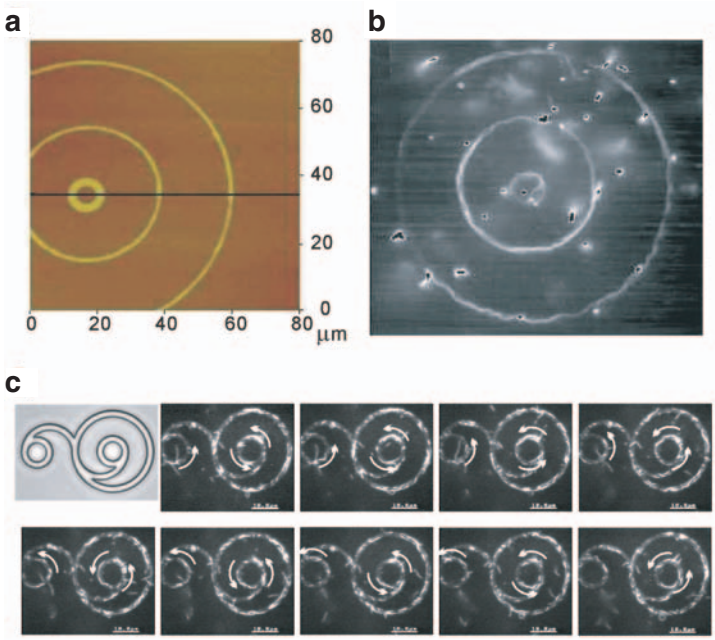

Fig. 3.7. (**a**) Atomic force micrograph of triple concentric circular PMMA tracks. (**b**) Fluorescence microscope images of actin filaments moving on PMMA tracks coated with myosin HMM molecules. The superpositioning of image at different time points shows that the movement of actin filaments is restricted to the tracks. (**c**) Extraction of unidirectional movement of actin filaments on HMM-coated PMMA tracks. The *first panel* shows a bright-field image of circular PMMA tracks. The fluorescence microscope images show actin filaments moving counter-clockwise along the tracks and being directed towards the smaller circular tracks

adding arrowhead patterns on the tracks [50]. Most microtubules entering the arrowheads against the direction in which the arrowheads points are induced to make an 180° turn (Fig. 3.8). As a result, unidirectional movement is generated by the rectifying action of the arrow-headed pattern. Precise analyses and design of these rectifiers has been carried out by [71]. Arrowhead rectifiers have enabled us to construct microminiaturized circulators, in which populations of microtubules rotate in one direction and transport materials on the micrometer scale in a predefined fashion.

In addition to the spatial control of the movement of protein filaments, the temporal control of motor protein activity has been investigated. Rapidly chasing the buffer solution with a new one is the simplest way to control the activity of motor proteins. Flushing out ATP induces rapid cessation of protein filament movement. To control the concentration of ATP, photoactivatable ATP is an alternative method. Kaplan and coworkers showed that light-induced activation of caged complexes can control the activity of

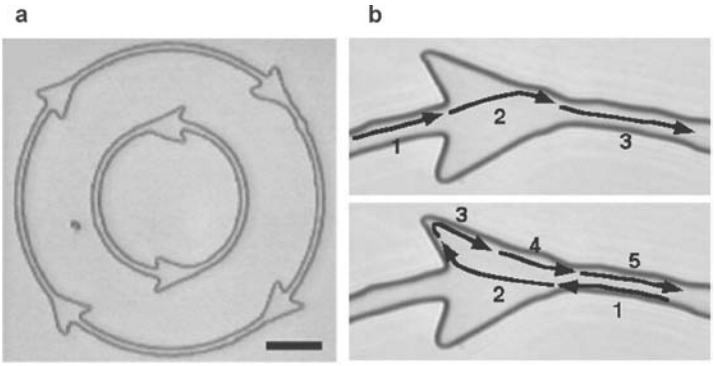

Fig. 3.8. Micro-fabricated circular grooves with arrowhead patterns to extract unidirectional movement from bi-directional, rotational movement of microtubules. (**a**) An optical microscopic image of the grooves. With this pattern, microtubules in the *outer circle* are moving clockwise, while those in the *inner circle* are moving counter-clockwise. (**b**) Schematic diagram of the arrowhead functioning as a rectifier of microtubule movement

proteins [52]. Caged nucleotides have been commonly used not only for the study of motor protein function [53] but also for controlling motor proteins in nanomachine-development [54]. One promising approach to controlling the activity of motor proteins is the development of caged proteins pioneered by G. Marriott [55, 56]. Caged heavy meromyosin was prepared by conjugating the thiol reactive reagent 1-(bromomethyl)-2-nitro-4, 5-dimethoxybenzene with the critical thiol group in the so-called SH1-helix. This treatment renders the molecule inactive. It can be reactivated by a pulse of near-ultraviolet light. Following irradiation with UV light, actin filaments on HMM-coated surface concomitantly start to move with velocities comparable to those of unmodified HMM [55].

On the other hand, the fast and reversible on- and off-switching of the motile activity of motor proteins needs to be investigated for the application of motor proteins to nanomachines. Rapid perturbation such as a temperature jump can be used to control movement of protein filaments. Kato et al., developed a temperature-pulse microscope in which an IR laser beam locally illuminated an aggregate of metal particles bound on a surface [57]. Using this system, the temperature of a microscopic region of ca. 10 μm in diameters was raised reversibly in a square-wave fashion with rise and fall times of several ms with a temperature gradient up to 2 degrees C/micrometer. Using an in vitro motility assay, they showed that the motor functions can be thermally and reversibly activated even at temperatures that are high enough to normally damage the proteins. By combining directional control of movement of protein filaments with this temperature jump method or application of light, external electric and magnetic fields, it should be possible to control cargo loading and unloading as well as the motor protein activities.

Controlling the position and orientation of motor proteins with subnanometer precision constitutes another key technology: motor proteins need to be placed with nanometer accuracy on a surface and their orientation controlled within a few degrees. Spudich and coworkers demonstrated that HMM molecules, sterospecifically bound to a single actin filament in rigor, could be transferred to nitrocellulose-coated surface by addition of ATP and that transferred HMM supported motility of actin filaments [58]. Combining this technique to filament-alignment techniques may provide a surface on which motor proteins are aligned with high spatial precisions and orientation.

Several methods for coupling motor proteins to the surface have been reported. Fusion motor proteins with bacterial biotin-binding proteins can bind specifically to streptavidin-coated cargoes or surfaces. Many peptide tags fused to expressed proteins have been commonly used to make the purifications easy. Some of these tags were used to couple the proteins to surfaces coated with the complementary ligand or antibodies [59–61].

3.9 Conclusions and Perspectives

Here, we have described the basic properties of motor proteins and how molecular biological techniques can be used to generate recombinant motors with well defined properties. The alignment of motor proteins and cytoskeletal filaments while maintaining their functions has been achieved by the use of nano- and micro-fabrication techniques. The methods described here are useful for establishing micrometer- or nanometer-scale arrays of motor proteins and filaments, and straightforward in their application. The use of motor proteins in nanometric actuators is moving a step closer towards realization. The generation of backwards- and forwards-moving motors that display increased thermal stability, optimized kinetic properties, and tight regulation by external signals will play an important part in the integration of biomolecules into nanotechnological devices.

The mechanochemical coupling in myosin, as described here, is a paradigm for linear motor proteins in general and suggests that the activity of these nanomachines can be mediated or regulated by divers mechanisms. The occurrence of myosins with lever arms of different length constitutes a simple means of increasing the size of the working stroke and thereby the velocity [23]. Similarly, the angle through which the lever arm swings affects the size of the working stroke and velocity. It has been shown that the lever arm of class I myosins swings though a $\sim 30^\circ$ larger angle than in conventional myosin [34]. Fine-tuning of the rate of ATP turnover provides another way to modulate the velocity of motor proteins. This can be done by changing the rate of the ATP hydrolysis step or by modification of the rate of product release [62]. As the release of the hydrolysis products is greatly accelerated by actin-binding, modulation of the interaction with actin provides one means to affect motor function. In the case of some unconventional myosins, phosphorylation of a so-called "TEDS-residue" is required for normal coupling

between the actin and nucleotide bindings sites [63–65]. The negative charge introduced by the phosphate group stabilizes the rigor complex by reducing the dissociation rate constant more than 30-fold. Product inhibition by ADP provides another means to reduce the velocity of the motor protein. Mg^{2+}-ions, which act more like catalysts during the ATPase cycle, can affect the rate of ADP-release. For class-I and class-V myosins, it has been shown that changes in the concentration of free Mg^{2+}-ions within the physiological range affect velocity [63,66]. Motor activity can also be modulated by changes in the stiffness of the lever arm. The Ca^{2+}-ion dependent binding of light chains can induce such changes. Direct mechanical coupling between the heads of kinesin or myosin heavy chain dimers provides a further way to modulate motor activity and, with appropriate tuning of the hydrolysis and product release steps, can play a key role in the generation of processive motors and the directional movement of motor proteins in the absence of a stiff lever arm [67–69].

Acknowledgements

We thank E. Mandelkow and A. Marx for providing Fig. 3.1b. The work was supported by Special Coordination Funds for Promoting Science and Technology, the Ministry of Education, Culture, Sports, Science and Technology (K.O.); Fond der Chemischen Industrie and DFG grants MA1081/5-3 and MA1081/6-1 (D.J.M.).

References

1. R. D. Vale (2000). AAA proteins. Lords of the ring. *J Cell Biol*, **150**, pp. 13–20.
2. L. M. DiBella and S. M. King (2001). Dynein motors of the Chlamydomonas flagellum. *Int Rev Cytol*, **210**, pp. 227–268.
3. I. Milisav (1998). Dynein and dynein-related genes. *Cell Motil Cytoskeleton*, **39**, pp. 261–272.
4. M. P. Koonce and M. Samso (2004). Of rings and levers: the dynein motor comes of age. *Trends Cell Biol*, **14**, pp. 612–619.
5. D. J. Asai and M. P. Koonce (2001). The dynein heavy chain: structure, mechanics and evolution. *Trends Cell Biol*, **11**, pp. 196–202.
6. K. Oiwa and H. Sakakibara (2005). Recent progress in dynein structure and mechanism. *Curr Opin Cell Biol*, **17**, pp. 98–103.
7. M. A. Geeves, R. Fedorov, and D. J. Manstein (2005). Molecular mechanism of actomyosin-based motility. *Cell Mol Life Sci*, **62**, pp. 1462–1477.
8. S. A. Burgess, M. L. Walker, H. Sakakibara, P. J. Knight, and K. Oiwa (2003). Dynein structure and power stroke. *Nature*, **421**, pp. 715–718.
9. F. Kozielski, S. Sack, A. Marx, M. Thormahlen, E. Schonbrunn, V. Biou, A. Thompson, E. M. Mandelkow, and E. Mandelkow (1997). The crystal structure of dimeric kinesin and implications for microtubule-dependent motility. *Cell*, **91**, pp. 985–994.

10. F. J. Kull, E. P. Sablin, R. Lau, R. J. Fletterick, and R. D. Vale (1996). Crystal structure of the kinesin motor domain reveals a structural similarity to myosin. *Nature*, **380**, pp. 550–555.
11. I. Rayment, W. R. Rypniewski, K. Schmidt-Base, R. Smith, D. R. Tomchick, M. M. Benning, D. A. Winkelmann, G. Wesenberg, and H. M. Holden (1993). Three-dimensional structure of myosin subfragment-1: a molecular motor. *Science*, **261**, pp. 50–58.
12. R. S. Goody and W. Hofmann-Goody (2002). Exchange factors, effectors, GAPs and motor proteins: common thermodynamic and kinetic principles for different functions. *Eur Biophys J*, **31**, pp. 268–274.
13. R. D. Vale (1996). Switches, latches, and amplifiers: common themes of G proteins and molecular motors. *J Cell Biol*, **135**, pp. 291–302.
14. M. Anson, M. A. Geeves, S. E. Kurzawa, and D. J. Manstein (1996). Myosin motors with artificial lever arms. *EMBO J*, **15**, pp. 6069–6074.
15. T. Q. Uyeda, P. D. Abramson, and J. A. Spudich (1996). The neck region of the myosin motor domain acts as a lever arm to generate movement. *Proc Natl Acad Sci USA*, **93**, pp. 4459–4464.
16. P. B. Conibear, C. R. Bagshaw, P. G. Fajer, M. Kovacs, and A. Malnasi-Csizmadia (2003). Myosin cleft movement and its coupling to actomyosin dissociation. *Nat Struct Biol*, **10**, pp. 831–835.
17. P. D. Coureux, A. L. Wells, J. Menetrey, C. M. Yengo, C. A. Morris, H. L. Sweeney, and A. Houdusse (2003). A structural state of the myosin V motor without bound nucleotide. *Nature*, **425**, pp. 419–423.
18. T. F. Reubold, S. Eschenburg, A. Becker, F. J. Kull, and D. J. Manstein (2003). A structural model for actin-induced nucleotide release in myosin. *Nat Struct Biol*, **10**, pp. 826–830.
19. K. C. Holmes, I. Angert, F. J. Kull, W. Jahn, and R. R. Schroder (2003). Electron cryo-microscopy shows how strong binding of myosin to actin releases nucleotide. *Nature*, **425**, pp. 423–427.
20. H. Brzeska, T. J. Lynch, and E. D. Korn (1988). Localization of the actin-binding sites of Acanthamoeba myosin IB and effect of limited proteolysis on its actin-activated Mg2+-ATPase activity. *J Biol Chem*, **263**, pp. 427–435.
21. M. A. Geeves and P. B. Conibear (1995). The role of three-state docking of myosin S1 with actin in force generation. *Biophys J*, **68**, pp. 194S–199S; discussion 199S–201S.
22. K. Ito, T. Kashiyama, K. Shimada, A. Yamaguchi, J. Awata, Y. Hachikubo, D. J. Manstein, and K. Yamamoto (2003). Recombinant motor domain constructs of Chara corallina myosin display fast motility and high ATPase activity. *Biochem Biophys Res Commun*, **312**, pp. 958–964.
23. C. Ruff, M. Furch, B. Brenner, D. J. Manstein, and E. Meyhofer (2001). Single-molecule tracking of myosins with genetically engineered amplifier domains. *Nat Struct Biol*, **8**, pp. 226–229.
24. M. Tominaga, H. Kojima, E. Yokota, H. Orii, R. Nakamori, E. Katayama, M. Anson, T. Shimmen, and K. Oiwa (2003). Higher plant myosin XI moves processively on actin with 35 nm steps at high velocity. *EMBO J*, **22**, pp. 1263–1272.
25. S. Higashi-Fujime, R. Ishikawa, H. Iwasawa, O. Kagami, E. Kurimoto, K. Kohama, and T. Hozumi (1995). The fastest actin-based motor protein from the green algae, Chara, and its distinct mode of interaction with actin. *FEBS Lett*, **375**, pp. 151–154.

26. R. A. Walker (1995). ncd and kinesin motor domains interact with both alpha- and beta-tubulin. *Proc Natl Acad Sci USA*, **92**, pp. 5960–5964.
27. S. A. Endow, S. J. Kang, L. L. Satterwhite, M. D. Rose, V. P. Skeen, and E. D. Salmon (1994). Yeast Kar3 is a minus-end microtubule motor protein that destabilizes microtubules preferentially at the minus ends. *EMBO J*, **13**, pp. 2708–2713.
28. J. Menetrey, A. Bahloul, A. L. Wells, C. M. Yengo, C. A. Morris, H. L. Sweeney, and A. Houdusse (2005). The structure of the myosin VI motor reveals the mechanism of directionality reversal. *Nature*, **435**, pp. 779–785.
29. A. L. Wells, A. W. Lin, L. Q. Chen, D. Safer, S. M. Cain, T. Hasson, B. O. Carragher, R. A. Milligan, and H. L. Sweeney (1999). Myosin VI is an actin-based motor that moves backwards. *Nature*, **401**, pp. 505–508.
30. A. Inoue, J. Saito, R. Ikebe, and M. Ikebe (2002). Myosin IXb is a single-headed minus-end-directed processive motor. *Nat Cell Biol*, **4**, pp. 302–306.
31. M. A. Geeves, and K. C. Holmes (1999). Structural mechanism of muscle contraction. *Ann Rev Biochem*, **68**, pp. 687–728.
32. G. Tsiavaliaris, S. Fujita-Becker, and D. J. Manstein (2004). Molecular engineering of a backwards-moving myosin motor. *Nature*, **427**, pp. 558–561.
33. W. Kliche, S. Fujita-Becker, M. Kollmar, D. J. Manstein, and F. J. Kull (2001). Structure of a genetically engineered molecular motor. *EMBO J*, **20**, pp. 40–46.
34. M. Kollmar, U. Dürrwang, W. Kliche, D. J. Manstein, and F. J. Kull (2002). Crystal structure of the motor domain of a class-I myosin. *EMBO J*, **21**, pp. 2517–2525.
35. B. Prakash, L. Renault, G. J. Praefcke, C. Herrmann, and A. Wittinghofer (2000). Triphosphate structure of guanylate-binding protein 1 and implications for nucleotide binding and GTPase mechanism. *EMBO J*, **19**, pp. 4555–4564.
36. S. J. Kron and J. A. Spudich (1986). Fluorescent actin filaments move on myosin fixed to a glass surface. *Proc Natl Acad Sci USA*, **83**, pp. 6272–6276.
37. L. Limberis and R. J. Stewart (2000). Toward kinesin-powered microdevices. *Nanotechnol*, **11**, pp. 47–51.
38. R. Stracke, K. J. Bohm, J. Burgold, H. J. Schacht, and E. Unger (2000). Physical and technical parameters determining the functioning of a kinesin-based cell-free motor system. *Nanotechnol*, **11**, pp. 52–56.
39. K. J. Böhm, R. Stracke, P. Muhlig, and E. Unger (2001). Motor protein-driven unidirectional transport of micrometer-sized cargoes across isopolar microtubule arrays. *Nanotechnol*, **12**, pp. 238–244.
40. R. Bunk, J. Klinth, L. Montelius, I. A. Nicholls, P. Omling, S. Tagerud, and A. Mansson (2003). Actomyosin motility on nanostructured surfaces. *Biochem Biophys Res Commun*, **301**, pp. 783–788.
41. D. V. Nicolau, H. Suzuki, S. Mashiko, T. Taguchi, and S. Yoshikawa (1999). Actin motion on microlithographically functionalized myosin surfaces and tracks. *Biophys J*, **77**, pp. 1126–1134.
42. H. Suzuki, A. Yamada, K. Oiwa, H. Nakayama, and S. Mashiko (1997). Control of actin moving trajectory by patterned poly(methylmethacrylate) tracks. *Biophys J*, **72**, pp. 1997–2001.
43. H. Suzuki, K. Oiwa, A. Yamada, H. Sakakibara, H. Nakayama, and S. Mashiko (1995). Linear Arrangement of Motor Protein on a Mechanically Deposited Fluoropolymer Thin Film. *Jpn J Appl Phys*, **34**, pp. 3937–3941.

44. J. C. Wittmann and P. Smith (1991). Highly oriented thin-films of poly(tetrafluoroethylene) as a substrate for oriented growth of materials. *Nature*, **352**, pp. 414–417.
45. D. Fenwick, P. Smith, and J. C. Wittmann (1996). Epitaxial and graphoepitaxial growth of materials on highly orientated PTFE substrates. *J Mat Science*, **31**, pp. 128–131.
46. J. R. Dennis, J. Howard, and V. Vogel (1999). Molecular shuttles: directed motion of microtubules slang nanoscale kinesin tracks. *Nanotechnol*, **10**, pp. 232–236.
47. K. Oiwa, D. M. Jameson, J. C. Croney, C. T. Davis, J. F. Eccleston, and M. Anson (2003). The 2′-O- and 3′-O-Cy3-EDA-ATP(ADP) complexes with myosin subfragment-1 are spectroscopically distinct. *Biophys J*, **84**, pp. 634–642.
48. J. Clemmens, H. Hess, J. Howard, and V. Vogel (2003a). Analysis of microtubule guidance in open microfabricated channels coated with the motor protein kinesin. *Langmuir*, **19**, pp. 1738–1744.
49. J. Clemmens, H. Hess, R. Lipscomb, Y. Hanein, K. F. Bohringer, C. M. Matzke, G. D. Bachand, B. C. Bunker, and V. Vogel (2003b). Mechanisms of microtubule guiding on microfabricated kinesin-coated surfaces: Chemical and topographic surface patterns. *Langmuir*, **19**, pp. 10967–10974.
50. Y. Hiratsuka, T. Tada, K. Oiwa, T. Kanayama, and T. Q. Uyeda (2001). Controlling the direction of kinesin-driven microtubule movements along microlithographic tracks. *Biophys J*, **81**, pp. 1555–1561.
51. R. Bunk, M. Sundberg, A. Mansson, I. A. Nicholls, P. Omling, S. Tagerud, and L. Montelius (2005). Guiding motor-propelled molecules with nanoscale precision through silanized bi-channel structures. *Nanotechnol*, **16**, pp. 710–717.
52. J. H. Kaplan, B. Forbush, 3rd, and J. F. Hoffman (1978). Rapid photolytic release of adenosine 5′-triphosphate from a protected analogue: utilization by the Na:K pump of human red blood cell ghosts. *Biochemistry*, **17**, pp. 1929–1935.
53. J. A. McCray, L. Herbette, T. Kihara, and D. R. Trentham (1980). A new approach to time-resolved studies of ATP-requiring biological systems; laser flash photolysis of caged ATP. *Proc Natl Acad Sci USA*, **77**, pp. 7237–7241.
54. H. Hess, J. Clemmens, D. Qin, J. Howard, and V. Vogel (2001). Light-controlled molecular shuttles made from motor proteins carrying cargo on engineered surfaces. *Nano Letters*, **1**, pp. 235–239.
55. G. Marriott and M. Heidecker (1996). Light-directed generation of the actin-activated ATPase activity of caged heavy meromyosin. *Biochemistry*, **35**, pp. 3170–3174.
56. G. Marriott, P. Roy, and K. Jacobson (2003). Preparation and light-directed activation of caged proteins. *Methods Enzymol*, **360**, pp. 274–288.
57. H. Kato, T. Nishizaka, T. Iga, K. Kinosita, Jr., and S. Ishiwata (1999). Imaging of thermal activation of actomyosin motors. *Proc Natl Acad Sci USA*, **96**, pp. 9602–9606.
58. Y. Y. Toyoshima, C. Toyoshima, and J. A. Spudich (1989). Bidirectional movement of actin filaments along tracks of myosin heads. *Nature*, **341**, pp. 154–156.
59. Y. Inoue, Y. Y. Toyoshima, A. H. Iwane, S. Morimoto, H. Higuchi, and T. Yanagida (1997). Movements of truncated kinesin fragments with a short or an artificial flexible neck. *Proc Natl Acad Sci USA*, **94**, pp. 7275–7280.

60. S. Itakura, H. Yamakawa, Y. Y. Toyoshima, A. Ishijima, T. Kojima, Y. Harada, T. Yanagida, T. Wakabayashi, and K. Sutoh (1993). Force-generating domain of myosin motor. *Biochem Biophys Res Commun*, **196**, pp. 1504–1510.
61. A. H. Iwane, K. Kitamura, M. Tokunaga, and T. Yanagida (1997). Myosin subfragment-1 is fully equipped with factors essential for motor function. *Biochem Biophys Res Commun*, **230**, pp. 76–80.
62. R. W. Lymn and E. W. Taylor (1970). Transient state phosphate production in the hydrolysis of nucleoside triphosphates by myosin. *Biochemistry*, **9**, pp. 2975–2983.
63. S. Fujita-Becker, U. Dürrwang, M. Erent, R. J. Clark, M. A. Geeves, and D. J. Manstein (2005). Changes in Mg^{2+} ion concentration and heavy chain phosphorylation regulate the motor activity of a class I myosin. *J Biol Chem*, **280**, pp. 6064–6071.
64. E. M. Ostap, T. Lin, S. S. Rosenfeld, and N. Tang (2002). Mechanism of regulation of Acanthamoeba myosin-IC by heavy-chain phosphorylation. *Biochemistry*, **41**, pp. 12450–12456.
65. Z. Y. Wang, F. Wang, J. R. Sellers, E. D. Korn, and J. A. Hammer, 3rd (1998). Analysis of the regulatory phosphorylation site in Acanthamoeba myosin IC by using site-directed mutagenesis. *Proc Natl Acad Sci USA*, **95**, pp. 15200–15205.
66. S. S. Rosenfeld, A. Houdusse, and H. L. Sweeney (2005). Magnesium regulates ADP dissociation from myosin V. *J Biol Chem*, **280**, pp. 6072–6079.
67. N. J. Carter and R. A. Cross (2005). Mechanics of the kinesin step. *Nature*, **435**, pp. 308–12.
68. P. B. Conibear and M. A. Geeves (1998). Cooperativity between the two heads of rabbit skeletal muscle heavy meromyosin in binding to actin. *Biophys J*, **75**, pp. 926–937.
69. M. Nyitrai and M. A. Geeves (2004). Adenosine diphosphate and strain sensitivity in myosin motors. *Philos Trans R Soc Lond B Biol Sci*, **359**, pp. 1867–1877.
70. D. C. Turner, C. Chang, K. Fang, S. L. Brandow, and D. B. Murphy (1995). Selective adhesion of functional microtubules to patterned silane surfaces. *Biophys. J*, **69**, pp. 2782–2789.
71. M. G. L. van den Heuvel, C. T. Butcher, R. M. M. Smeets, S. Diez, and C. Dekker (2005). High rectifying efficiencies of microtubule motility on kinesin-coated gold nanostructures. *Nano Letters*, **5**, pp. 1117–1122.